ENGINE SURGE SIMULATION IN WIND-TUNNEL MODEL INLET DUCTS

K.W. Lotter
Messerschmitt-Boelkow-Blohm GmbH
Federal Republic of Germany

P.-A. Mackrodt
DFVLR Göttingen
Federal Republic of Germany

R.D. Scherbaum
Messerschmitt-Boelkow-Blohm GmbH
Federal Republic of Germany

Abstract

Engine surges are associated with one or more heavy pressure pulses, generally known as hammer shock. The peak pressure of this pulse ahead of the engine following an engine surge can exceed the total pressure in the inlet by a wide margin and, therefore, represents the critical load for the intake structure. Accurate knowledge about this pressure and its amplification and/or attenuation within the air inlet is essential for determining the structural requirements for the inlet. The complexity of this phenomenon means that it is difficult to make a purely theoretical prediction of the intake pressures during a surge and the designer is forced to rely largely on experimental data.

To simulate the engine surge pulses on a scaled intake wind-tunnel model a surge wave generator (SWG) was developed and calibrated. The SWG was installed in the intake duct downstream of the instrumented aerodynamic interface plane. The pressure wave to simulate the hammer shock was created by causing air to be blown intermittently upstream through a slot in a rotating hollow cylinder. By variation of slot blowing pressure, slot geometry and cylinder rotation speed the pressure signature produced in the intake could be influenced and a great similarity to the true surge pressure signature, measured during real engine surges was thus achieved. The SWG in its final configuration allowed the simulation of single (pop surge) and cyclic pressure waves (lock-in surge).

The SWG was installed and successfully used on a 1:10 scale intake wind tunnel model. The configuration represented was a fighter aircraft with twin side-by-side mounted belly intakes. The model was instrumented with 421 steady-state and 30 dynamic pressure probes. Tests were carried out statically and in the transonic and supersonic speed ranges up to $M_o = 2.0$.

Typical results of the time-variant pressures at various locations in the primary and secondary intake ducts are presented. The data served as a sound basis for dynamic load assessment in the intake and on its adjacent structure and for the prediction of time-variant total pressure distortion in the receiving (secondary) intake.

Notations

AIP	aerodynamic interface plane	
$\frac{a}{b}$	aspect ratio of intake duct panel	-
ETG	calibration tank (Eichtank Göttingen)	
$\frac{F}{F_{max}}$	Relative auxiliary air intake bracket force	-
f_{SWG}	frequency of surge pressure wave	Hz
M_o	free stream Mach number	-
p	static pressure	kPa
p_o	ambient pressure	kPa
p_1	static intake duct pressure at AIP	kPa
$p_{1\ max}$	maximum pressure of surge wave	kPa
$p_{1\ min}$	minimum pressure of surge wave	kPa
p_{SWG}	reverse flow blowing pressure	kPa
$\frac{p_{1\ max}}{p_1}$	overpressure ratio of surge wave	-
$\frac{p_2}{p_1}$	overall static engine compressor pressure ratio	-
QA	mass flow rate	$\frac{\sqrt{K}}{s}$
TWG	Transonic wind tunnel Göttingen	
t	time	s
t_1	surge wave rise time to max.press.	ms
t_2	time of positive surge wave	ms
t_3	time of first surge wave within a cyclic surge	ms

WAT_{EF}	corrected engine mass flow	$\frac{kg \cdot \sqrt{K}}{s \cdot kPa}$
X	aircraft station	mm
α	model angle of attack	deg
β	model angle of yaw	deg
Θ	auxiliary air intake door angle	rad
Θ_{VC}	intake vary-cowl angle	deg

1. INTRODUCTION

The aspect of intake/engine compatibility needs special consideration during the development of a new flight vehicle. This is especially true for supersonic fighter aircraft as the wide range of aircraft attitude and flight speed can cause flow distortions in the air intake at extreme flight conditions. As a result engine surges may be experienced. Great effort is generally undertaken to minimize intake flow distortions and/or to increase the engine tolerance to such distortions. Thus, the risk of surge for an operational fighter aircraft is low. However, the possibility of surges cannot be totally excluded since malfunctions of the intake or engine control and reheat overfuelling are further factors that possibly trigger surge.

Engine surges are associated with one or more heavy pressure pulses, generally known as hammer shock. The peak pressure of this pulse ahead of the engine following an engine surge can exceed the total pressure of the inlet by a wide margin and, therefore, represents the critical load for the intake structure. Accurate knowledge about this pressure and its amplification and/or attenuation within the air inlet is essential for determining the structural requirements for the inlet. There was a major structural failure, for example, during Concorde prototype flying when an intake ramp was even blown out due to underestimation of the differential pressures created across the ramp during an interactive surge of two adjacent propulsion systems.

The complexity of this phenomenon means that it is difficult to make a purely theoretical prediction of the intake pressures during a surge and the designer is forced to rely largely on available experimental data. Various correlations have been published for different engines (Ref. 1,2,3), but there is still a lack of generality because the peak pressure is not only dependent on the engine considered but also on the cause of the surge. Further variables influencing the surge pulse strength are engine inlet Mach number, fan bypass ratio and engine cycle pressure ratio. Most correlations to date have shown the peak surge pressure to be a function of overall compressor pressure ratio and bypass ratio, Fig. 1 (Ref. 3).

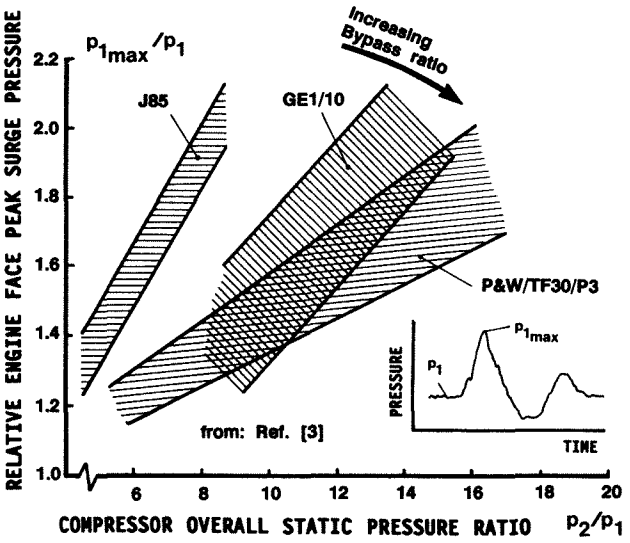

Fig. 1 Effect of compressor overall pressure ratio and bypass ratio on peak surge pressure

Even when the peak surge pressure ahead of the engine is known, estimating peak pressures along the intake duct and within the structure of the forward intake nacelle and bleed system as well as assessment of pressure pulse attenuation upstream of the intake entry plane is a difficult task.

A surge wave generator (SWG) was designed and developed with the aim of simulating the engine surge pressure pulses in a scaled intake wind-tunnel model and measuring the time-variant pressures at various locations on the intake nacelle and duct wall. This paper deals with the special features of this SWG, its development and its successful application on a 1:10 scale intake wind tunnel model.

2. CONSEQUENCES OF ENGINE SURGE

2.1 Dynamic loads in air intake

The sudden increase in the local static pressure created by the upstream surge wave propagation varies along the intake duct depending on the initial surge wave signature and on the duct area distribution. This increase can rise to considerable values in narrowing cavities like the bleed chamber above intake ramps in a wide slot bleed system as shown in Fig. 2. The data in this diagram was collected during a full scale Tornado intake/engine test in Cell 4 at NGTE Pyestock during supersonic speeds with distributed dynamic pressure measurement (Ref. 4).

Fig. 2 shows the forward intake and the duct together with the peak surge pressure rise along the duct (lower half of diagram), the local amplitude being referred to the amplitude at the engine face.

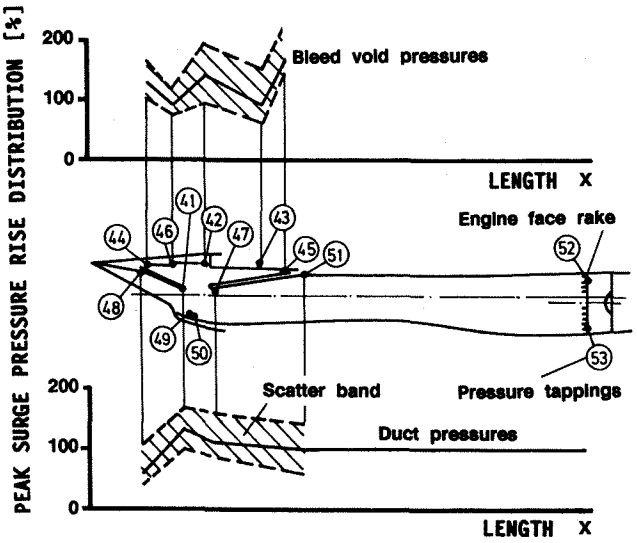

Fig. 2 Peak surge pressure rise distribution along intake duct (Tornado aircraft)

The pressure rise time associated with the surge is extremely short - in the order of 1 to 2 milliseconds. The sudden application of surge pressure can result in stress amplifications within the intake structure. In Fig. 3 the increased stress level expressed as a gain factor is clearly influenced by duct panel size, and correct sizing of the panel can lead to considerable reductions in stress.

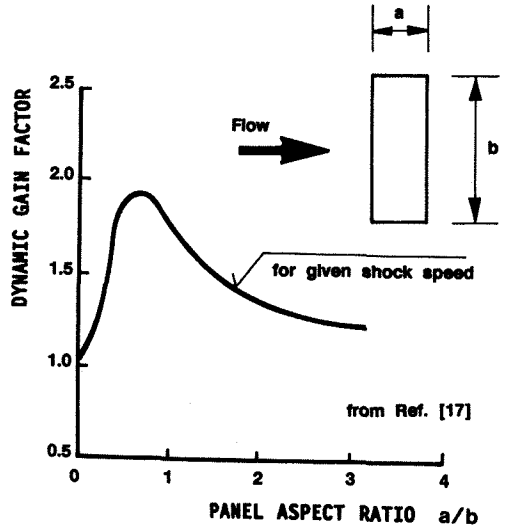

Fig. 3 Dynamic gain factor as function of intake duct panel aspect ratio

2.2 Structural failures

During early prototype flying with the Tornado fighter aircraft there were auxiliary air intake door failures due to excessive surge loads. These high loads were created by heavy surges following bird ingestion and reheat overfuelling. The damage occurred to the brackets linking the inner and outer doors, Fig. 4, see also Ref. (4). When the doors are partly or fully open, i.e. during high engine rating at low flight speed and on the ground respectively, the surge pressure can penetrate into the space between the doors and create high tension forces in the brackets (see Fig. 4). The magnitude of the peak pressure between the doors was underestimated during prototype design due to lack of data. For the production aircraft a redesign was incorporated with reinforcement of the relevant parts. This costly modification could certainly have been avoided if a suitable simulation of engine surge waves in a scaled intake wind-tunnel model had been performed. However, such a device was not available at that time.

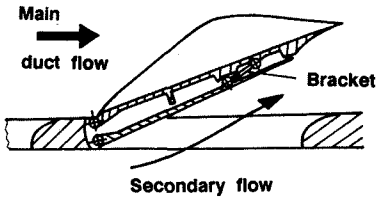

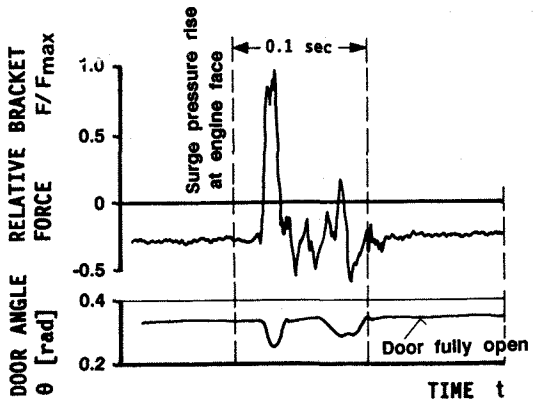

Fig. 4 Variation of bracket force in auxiliary air intake door during engine surge

3. REQUIREMENTS FOR SURGE SIMULATION ON INTAKE WIND-TUNNEL MODELS

From the facts described in the previous chapter it is evident that simulation of engine surge pressure waves in intake wind-tunnel models associated with the relevant dynamic pressure instrumentation would allow the assessment of dynamic pressure loads at an early stage in the development of a new aircraft. Before the development of such a surge wave generator (SWG) can be initiated typical engine surge pressure signatures as produced from a real engine have to be assessed. With the RB199 engine in the Tornado aircraft two typical surge types have been identified, Fig. 5:

- o lock-in surge (cyclic wave)
- o pop surge (single wave)

The lock-in surge creates a repetitive pressure wave as shown in the upper half of the diagram. Engine shut-down is required to terminate surging.

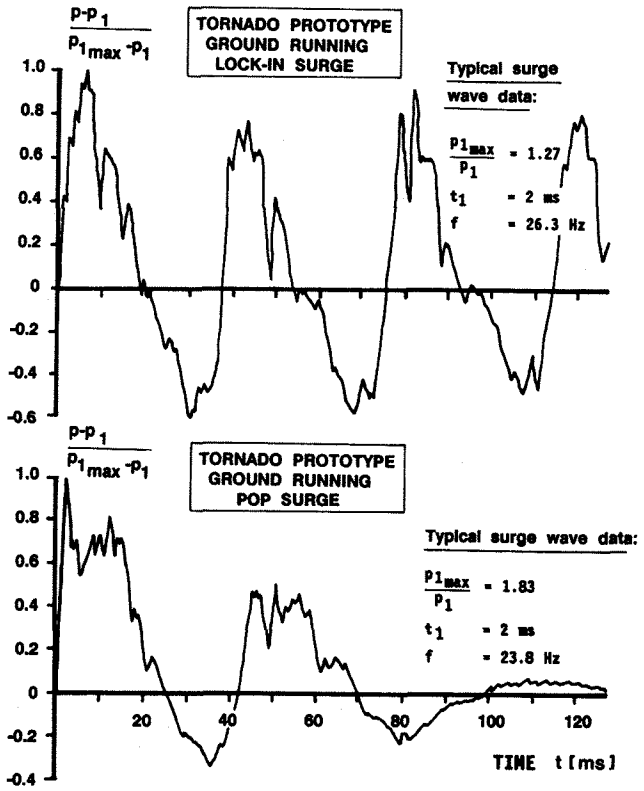

Fig. 5 Surge pressure signatures from RB 199 engine in Tornado aircraft

The pop surge is a single, self-recovering surge with one or two pressure pulses as shown on the lower diagram.

Both types of surge pressure signatures were measured at the duct wall just upstream of the engine face during ground running. Characteristic data obtained from these traces are:

	Overpressure	Rise time	Frequency of surge wave
	$\frac{p_{1max}}{p_1}$	t_1 [ms]	f [Hz]
Lock-in surge	1.27	2	26.3
Pop surge	1.83	2	23.8

This data served as the basis for the SWG development, which is described in chapter 4.

For simulation of these pressure waves the key parameters defining the surge pressure signature versus time were identified as shown in Fig. 6, i.e.

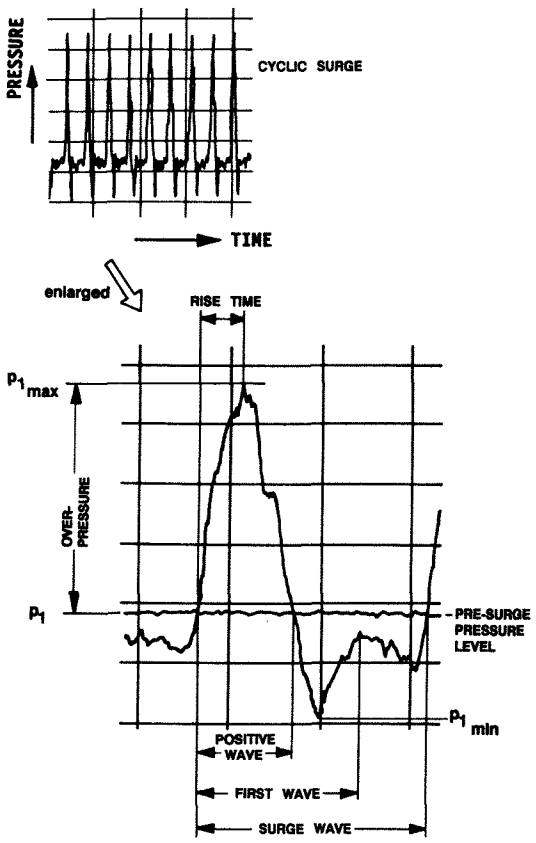

Fig. 6 Key parameters defining surge pressure signature

Maximum surge pressure	p_{1max}
Pre-surge pressure level (steady state static intake duct pressure)	p_1
Minimum surge pressure	p_{1min}
Rise time from steady state to peak level	t_1
Positive wave time	t_2
First wave time	t_3

On the basis of Fig. 5 and the data given in the table together with the fact that the SWG was to be installed in a 1:10 scale intake model with the possibility of varying some key surge parameters, the following requirements for a SWG were set up:

Overpressure ratio range	up to 2.0
Positive wave time	3 + 0.5 ms
Rise time	0,2 to 1.0 ms
First wave time	up to 4.5 ms
Surge wave frequency	160 to 280 Hz

4. DESIGN AND DEVELOPMENT OF A SURGE WAVE GENERATOR

4.1 Preliminary investigations

Before the development of the surge wave generator was initiated, preliminary investigations were carried out

- o to obtain insight into the mechanism of pressure wave propagation
- o to identify potential devices for surge simulation and
- o to select the most suitable device for further development.

4.1.1 Shock tunnel investigation

To obtain insight into the mechanism of pressure wave propagation a pilot test in the shock tunnel at the ISL (Institut Franco-Allemand de Recherches Saint Louis) was carried out (Ref. 5). The aim was to make a quantitative investigation of the upstream pressure wave propagation in a simulated intake duct, to investigate its diffraction at the forward end and its attenuation in an adjacent duct. The test set-up is shown in Fig. 7. Within the test section plenum a rectangular duct (38x50 mm) was installed. The rear part was divided into two ducts by a vertical splitter wall to simulate two adjacent intake ducts. One of these ducts was then blocked by a reflection plate. This plate was exchangeable to allow different degrees of blockage to be simulated by perforated plates.

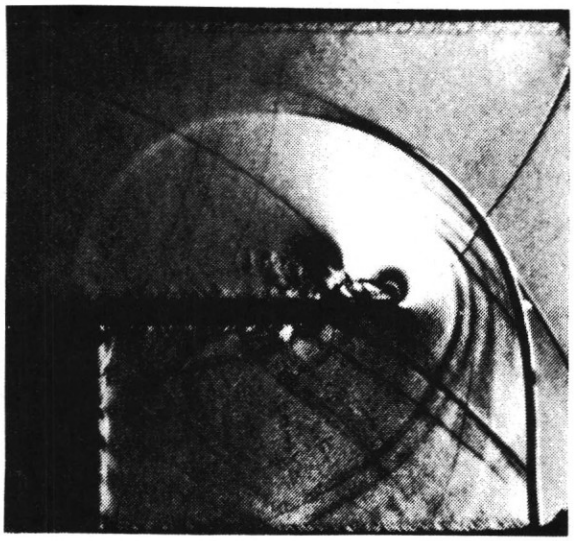

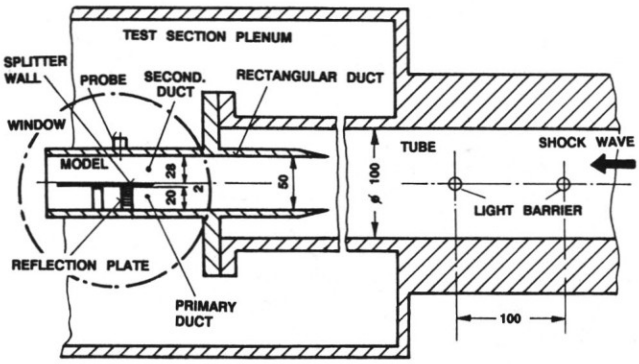

Fig. 7 Shock tunnel tests to simulate surge wave propagation in a twin duct

A test run is initiated by bursting the shock tube diaphragm. A shock then travels down the shock tube, its velocity being a function of the driver gas pressure and the speed of sound of both the driver and the test gas. Air was used as test gas and nitrogen or helium for the driver gas. The flow velocity behind the travelling shock can be either subsonic or supersonic, depending on the driver gas selected, its initial pressure and the initial shock tube pressure.

The flow behind the shock simulates the flow in an intake duct. After reflection of the shock at the reflection plate the shock travels backwards, thus bringing the flow in the simulated intake duct to rest. As the reflected shock reaches the leading edge of the splitter wall it is diffracted and spreads into the adjacent duct.

The flow conditions simulated in the shock tunnel are shown in the following table:

Shock Mach number	Flow Mach number	Initial shock tube pressure (bar)	Driver gas pressure ratio	Driver gas
1.5	0.6	1	2.46	N_2
1.6	0.7	1	2.82	N_2
3.5	1.6	0.067	14.6	He

The photograph in Fig. 7 (top) was taken just after the reflected shock had left the primary (lower) duct. The diffraction into the adjacent duct can be clearly seen. Shock Mach number was 1.5, flow Mach number 0.6 and the reflection plate was perforated with an open area ratio of 0.26 during this test.

The conditions in both the primary and secondary duct were measured not only by pressure sensors but also by "streak pictures" and Laser differential interferometry.

The pressure in the primary duct behind the reflected shock reached values comparable to those measured in an intake duct during an engine surge, suggesting that a proper simulation of a real surge was achieved. The measured pressure steps in the adjacent duct due to the diffracted shock were negligible, i.e. as low as 0 to 7% of the steady state static duct pressure.

4.1.2 BAe Filton investigations

In the 1960's the need arose to simulate the surge pressures of the Rolls Royce Olympus 593 engine in a Concorde air intake wind-tunnel model, an investigation to support intake development.

a) An early BAe Filton surge simulator used a rotating slotted valve intended for cyclic

surge simulation (see Fig. 8). When the valve was stationary, the intake mass flow passed straight through the open slots in the valve and the body. When the valve was rotating, it intermittently cut off the flow through the intake. Surge frequency, and to some extent rise time, were dependent on valve rotation speed. Rise time, and to some extent wave shape, depended on the relative variation of slot widths between valve and body. Not surprisingly, overpressure ratios were far too low.

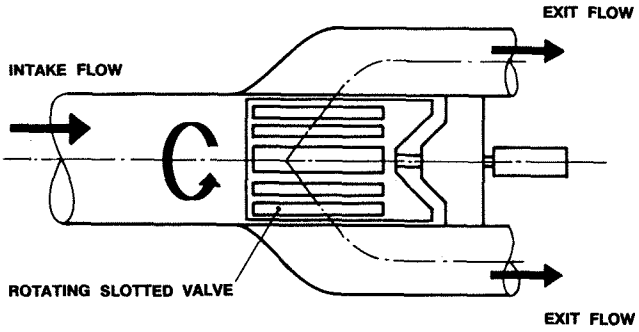

Fig. 8 Rotating slotted valve (BAe Filton)

b) BAe Filton also built and tested an early surge simulator, for single surge wave simulation, using a rifle breech mechanism as shown in Fig. 9. When the rifle was fired (using a blank cartridge of course) the explosive charge

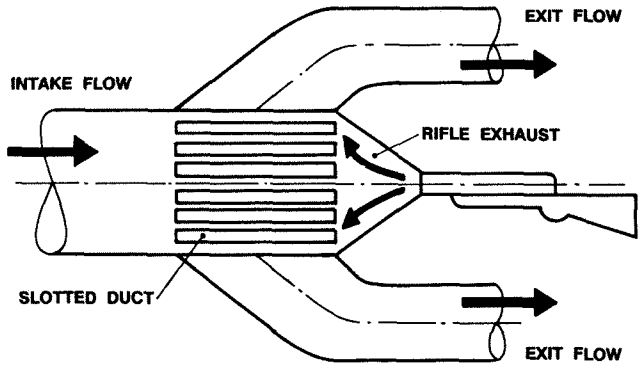

Fig. 9 Single surge simulation by rifle breech mechanism (BAe Filton)

injected a pressure wave into the intake duct against the main intake flow. A simulation of the correct overpressure was found to be possible, as well as a limited variation of the pulse shape by packing the explosive charge in different ways. However the rise time was far too short for the Olympus 593 engine simulated, even using a "low explosive" charge. Additional drawbacks were lack of reproducibility and potential damage to the engine face instrumentation ahead of the rifle breech.

c) The final BAe Filton surge simulator (Ref. 6) was for cyclic surge, and consisted of a cylinder with butterfly vanes which uncovered a forward-facing slot in its fixed hollow shaft at the same time as the main intake flow was shut off (see Fig. 10). A "slug" of compressed air was injected forward of the slot when the latter was uncovered.

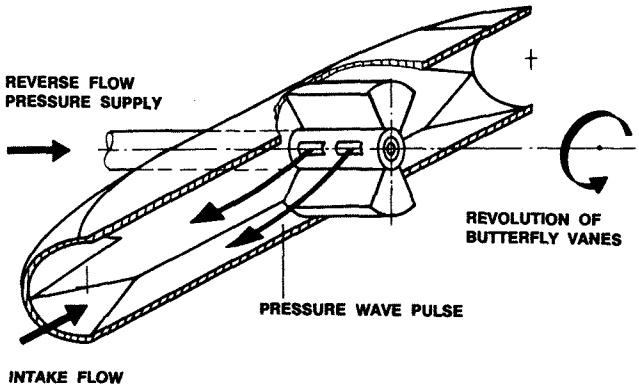

Fig. 10 Butterfly valve (BAe Filton)

It was possible to lock the butterfly valve in the fully open position for steady state intake testing. To minimise frontal areas in the wind tunnel, the rotating cylinder with vanes was driven by a small compressed air turbine. Rise time was dependent on valve rotation speed, relative widths of shaft and cylinder slots, and reverse flow pressure. Overpressure ratio was largely a function of reverse flow pressure. Surge frequency depended on valve rotation speed. It was possible to tune surge wave shape by changing the shape of the vane tips. The surge characteristics of the Olympus 593 were very well simulated, and this simulator was successfully used for Concorde intake surge interaction tests at supersonic speeds in the RAE 8ft tunnel at Bedford, United Kingdom.

In the 1970's a fighter aircraft proposal was made by MBB, known as TKF 90, with twin side by side intakes mounted under the fuselage (see Fig. 11). Surge simulation in one of the two intake ducts was envisaged on a 1:10 scale intake model. However, shorter pressure rise times and higher duct mass flows than in the Concorde tests were reqired.

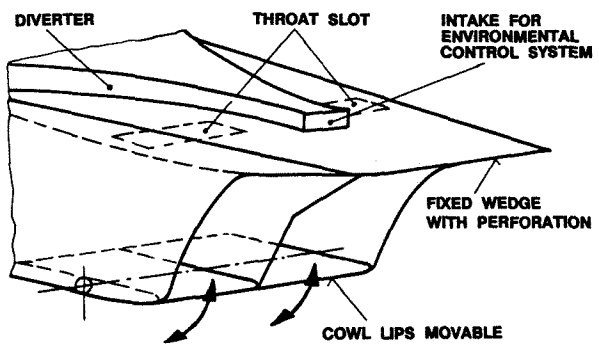

Fig. 11 MBB fighter intake concept for TKF 90

With the objective of further developping the surge simulator concept of BAe Filton to fulfil these new requirements, the existing butterfly valve was tested on a suction rig at BAe in early 1980. Initial guidelines for the further development have thus been worked out (Ref. 7).

Parallel to these activities, concept studies on alternative solutions for a SWG were carried out at MBB:

4.1.3 Rotating disc (Fig. 12)

In this concept a high pressure air tube enters the air intake duct from the side. The high pressure air is intermittently injected using a rotating disc system. Hole patterns in both the fixed and the rotating disc allow the high pressure air to pass the disc in the overlapping position. The pressure waves generated can be controlled by the disc hole pattern, the revolution speed and the supply pressure level.

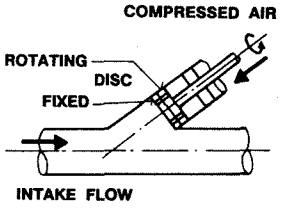

Fig. 12 Rotating disc concept

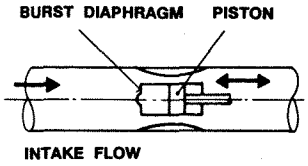

Fig. 13 Burst diaphragm

4.1.4 Burst diaphragm (Fig. 13)

Downstream of the engine face station a high pressure air reservoir is installed at the centre line of the air intake duct. The front end is closed by a diaphragm which bursts at a predetermined pressure level. The high pressure in the reservoir can be achieved either by a piston or by an air feed pipe. The surge wave shape can be modified by the pressure level and the related diaphragm as well as by the enclosed air volume.

4.2 Concept for Surge Wave Generator

Following the preliminary tests and concept studies, the final SWG concept to be realised was selected. The system chosen is shown in Fig. 14.

A rotating hollow cylinder having spanwise slots 180° apart rotates around a hollow shaft with a forward facing slot. The shaft is fed with high pressure air. At each full revolution of the rotating cylinder the shaft slot is uncovered twice thus producing upstream pressure waves in the intake duct. A balance wheel is mounted on the rotating cylinder to assure uniform rotation. Two air motors drive the rotating cylinder and the balance wheel via a toothed belt.

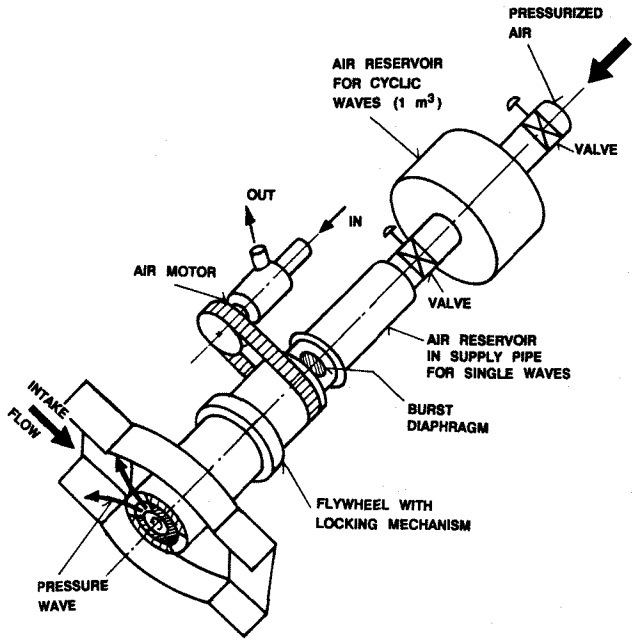

Fig. 14 System display of MBB surge wave generator

For the design of the SWG the following additional requirements were established:

- o no intake mass flow degradation due to installation of SWG, i.e. duct enlargement around rotating cylinder
- o no butterfly vanes (to avoid intake mass flow degradation during valve acceleration)
- o low maintenance to allow long-time operation in continuous wind tunnels
- o independent control of all SWG pressure supply systems
- o installation in a 1:10 scale intake model
- o single and cyclic pressure wave simulation

The types of pressure wave signatures which were to be simulated are shown in Fig. 15. Above

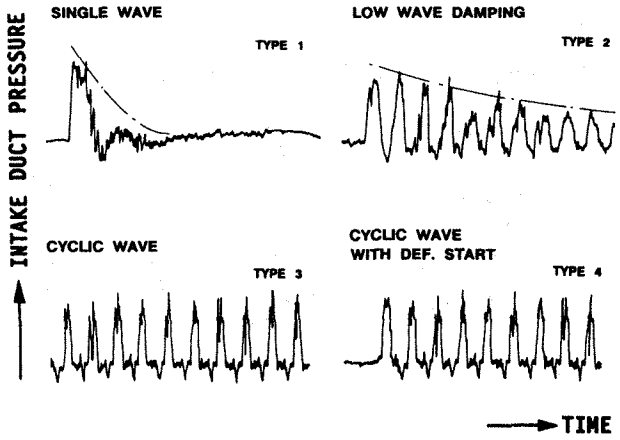

Fig. 15 Types of pressure wave signatures to be simulated

left a single wave with high damping representing a pop surge is shown (surge type 1). Above right a self-recovering surge with slow damping is represented (surge type 2). Surge type 3, below left, is a cyclic wave while surge type 4, below right, shows a cyclic wave with a defined starting point and the preceding steady-state condition. Both types 3 and 4 represent a lock-in engine surge which would require engine shut-down to recover.

To allow a single pressure wave (type 1) to be simulated a bursting diaphragm is installed in the supply pipe. The reverse flow in that case is supplied from the enclosed air reservoir within the SWG pressure pipe system, and the valve is locked in the open slot position. The diaphragm can be burst at a predetermined time by the actuation of a needle.

A low damping, type 2, was to be achieved by feeding the SWG from an enclosed volume of air but with the valve rotating, the wave damping being a function of the enclosed volume of air provided.

For continuous and stable air supply during cyclic surge wave simulation (type 4) a $1m^3$ air reservoir is installed. Type 3 is produced by a steady state reverse flow supply and a continuous rotation of the valve. For type 4 the reverse flow supply pipe is initially closed by the above-mentioned diaphragm with the pressure set at a given level while the valve is accelerated to the desired rotation speed. At a predetermined point in time the diaphragm is burst and the cyclic pressure wave is thus initiated.

4.3 Design and technical realization of the surge wave generator

The overall dimensions of the SWG case were defined by the 1:10 scale intake model to be used for these investigations (Ref. 8).

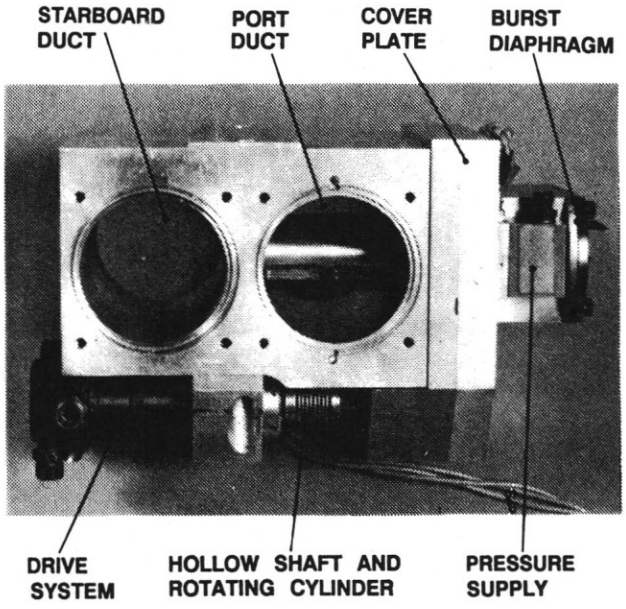

Fig. 16 Cross section of surge wave generator

The length was limited by the given location of the total pressure rake in the intake/engine aerodynamic interface plane (AIP) at the forward end and the throttle plug system at the rear end, see also section 5.3 and Fig. 33.

The front view of the SWG is shown in Fig. 16

The main components of the SWG are:

- o generator case
- o hollow shaft and rotating cylinder
- o burst diaphragm
- o drive system
- o pressure supply

The generator case (Fig. 17)

The generator case is manufactured from aluminium alloy. It can be installed between the total pressure rake and the throttle plug system of the wind tunnel model. Within that case the starboard intake duct has a constant diameter (since no surge device is installed there). The port duct diameter is enlarged in the region of the rotating cylinder to allow equal mass flows in both intake ducts. The outer side wall of the port duct is easily detachable for exchange of the hollow shaft and the rotating cylinder i.e. for slot shape variation and for maintenance of the bearings. This cover plate is made from steel to withstand the high pressure loads and to allow installation of the pressure supply pipe coupling mechanism as well as the diaphragm and the needle with actuator.

The instrumentation for counting the rotation speed of the valve is installed in the case to avoid any damage when making changes to the slot size configuration or when replacing the burst diaphragm.

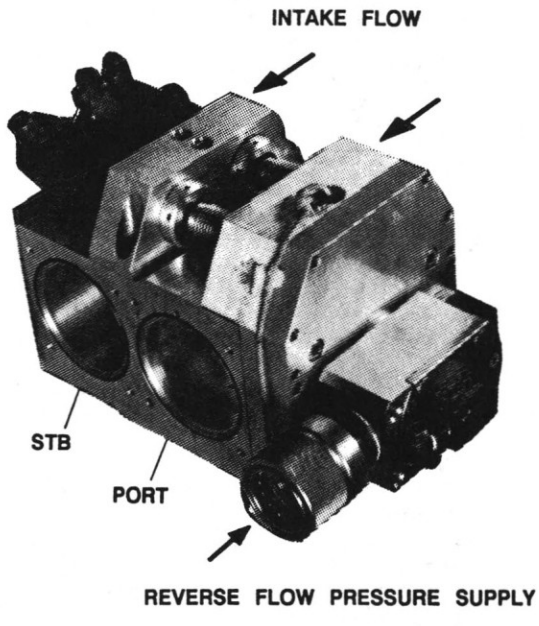

Fig. 17 Surge wave generator case

Fig. 18 shows the cover plate (shown turned by 90°) removed from the case. The hollow shaft, the rotating cylinder (removed) and the two air motors can be seen.

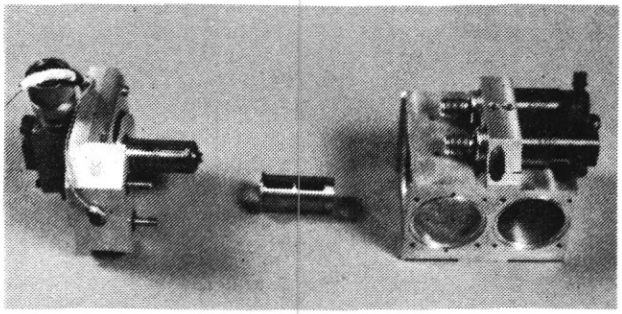

Fig. 18 Surge wave generator (dismounted)

The hollow shaft and rotating cylinder (Fig. 19)

The fixed shaft is hollow and has a spanwise slot at the forward side looking the opposite direction of the intake flow. A rotating hollow cylinder with two slots 180° apart rotates around that shaft. The bearings for the rotating cylinder are located in the splitter wall between the two intake ducts and in the cover plate respectively. They are fixed by a fixation cylinder which surrounds the rotating cylinder (see Fig. 19). A flywheel to equalize the rotation speed during cyclic loading is attached to the rotating cylinder.

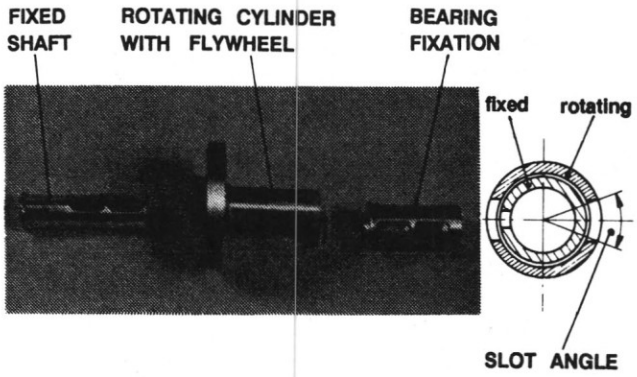

Fig. 19 Fixed hollow shaft and rotating cylinder with flywheel

The slot size is not varied in length but the opening angle ranges from 25° to 65°. Independent variation of slot sizes of the fixed shaft and rotating cylinder is possible to alter the pressure wave signature. The slot length is divided into two sections for strength reasons.

A pneumatic piston is installed in the cover plate to lock the flywheel in an open slot position for single pressure wave simulation with the burst diaphragm.

The burst diaphragm

A calibrated burst diaphragm is installed at the entry to the hollow shaft. Diaphragms with preselectable burst pressures ranging between 5 and 16 bar (± 10%) were chosen. A pointed needle can be actuated by a pneumatic piston to initiate bursting of the diaphragm at a predetermined point in time.

The driving system (Fig. 16 and 20)

The rotating cylinder together with the flywheel are driven by two air motors. Cogwheels and a toothed belt for power transmission are used. An inductive distance sensor is installed within the cover plate which senses the two cut-outs at the rim of the flywheel for revolution counting.

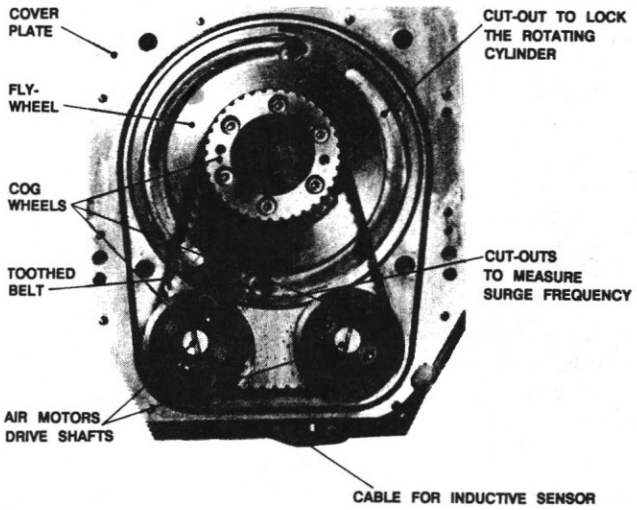

Fig. 20 Drive mechanism of surge wave generator

The pressure supply (Fig. 21)

Two pressure supply systems are used, one with 90 bar for SWG reverse flow and for the air motors, the other one with 8 bar for the pneumatic pistons which lock the flywheel and actuate the needle respectively.

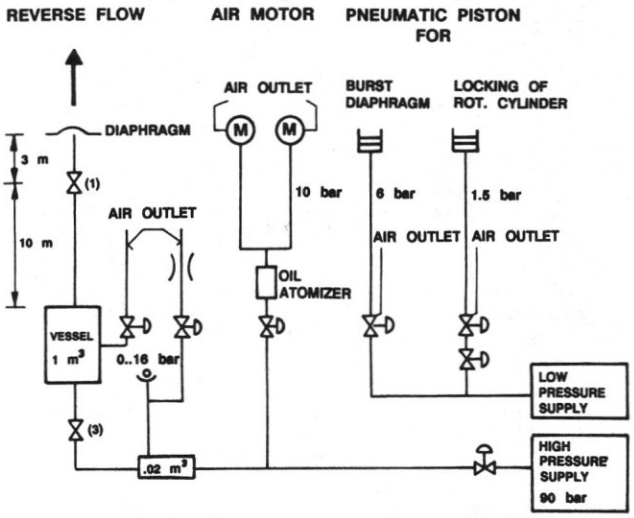

Fig. 21 Pressure supply system

For a single pressure wave simulation a volume of air with a pressure of up to 16 bar is enclosed between the burst diaphragm and a piston valve, see (1) in Fig. 21.

For the immediate start of a cyclic surge wave using the burst diaphragm the pressure control system was not fast enough to satisfy the rapid increase in the demand of air. Therefore, a large pressurized air vessel of 1 m^3 is installed close to the SWG. A pressure limiting valve keeps the pressure in the vessel below 16 bar. A remote-controlled air outlet system serves as a bypass when no reverse flow is demanded. By that means continuous air supply is maintained.

For the air motor the supply pressure is further reduced to 10 bar. An oil atomizer provides small amounts of oil for lubrication. The motor exhaust air is ducted out of the wind-tunnel test section.

A 6 bar pressure supply is used to operate the pneumatic piston of the SWG locking mechanism and a 1.5 bar supply to actuate the needle of the burst diaphragm. A bypass system is installed in the low pressure system too.

All pressure valves are remotely set and controlled from a control box connected to a computer (Fig. 22). Pressures are measured at various locations in the pipe system using strain gage transducers.

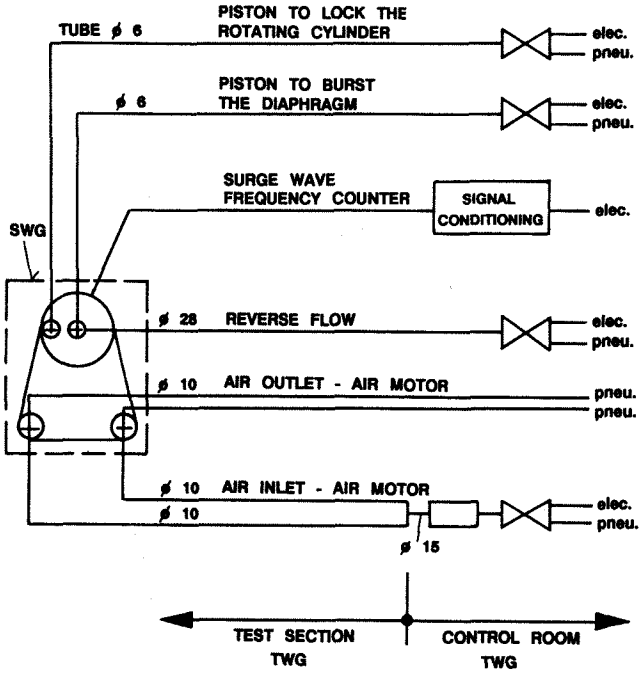

Fig. 22 Surge wave generator control system

4.4 Calibration procedure (Ref. 9, 10)

4.4.1 Calibration rig (Fig. 23)

The calibration tank at DFVLR Göttingen (ETG) was used, which provides a continuous suction mass flow at an accuracy of better than 0.3% (Ref. 14).

The SWG is attached to the front end of the calibration tank. The same arrangement as in the intake model is used, i.e. the rake at the aerodynamic interface plane and the intake duct are mounted in front of the SWG, the mass flow throttle plugs downstream of it. To avoid entry flow separation and the associated pressure losses a bell mouth replaces the intake nacelle.

An alternative configuration can be arranged with only a short duct and the bell mouth fitted in front of the AIP insert.

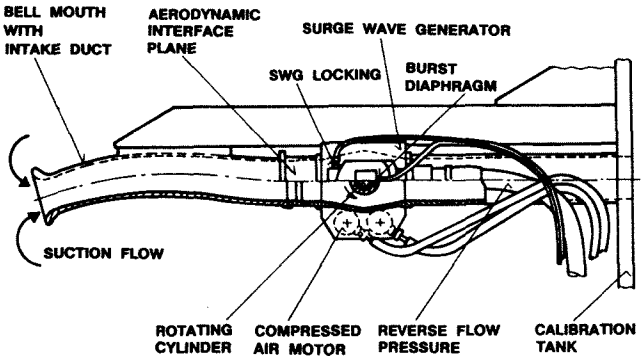

Fig. 23 Static calibration rig

During SWG calibration the surge wave types as described in section 4.2 were produced. For each run, the intake mass flow was varied from zero up to the maximum AIP Mach number.

The pressure wave signatures produced in the intake duct at the aerodynamic interface plane were digitized and stored on magnetic tape for later analysis.

4.4.2 Variation of test parameters

For a given intake/duct configuration the following parameters can be varied to influence the shape of the surge wave signature:

- o surge wave frequency f_{SWG}
- o slot angle of fixed shaft and rotating cylinder
- o reverse flow pressure p_{SWG}
- o intake mass flow rate QA

All these parameters were systematically varied during the SWG calibration procedure in order to assess their effect on the key parameters which define the surge wave signature. Working charts could then be established to enable the test engineer to select the relevant parameter setting when a given surge characteristic is to be simulated.

For a selected SWG configuration with long intake duct and without AIP rake Fig. 24 shows the effects of surge wave frequency, reverse flow pressure and slot angle on overpressure ratio, positive wave time and rise time for an intake mass flow rate of $QA = 0.32 \sqrt{K}/s$. As can be seen on the

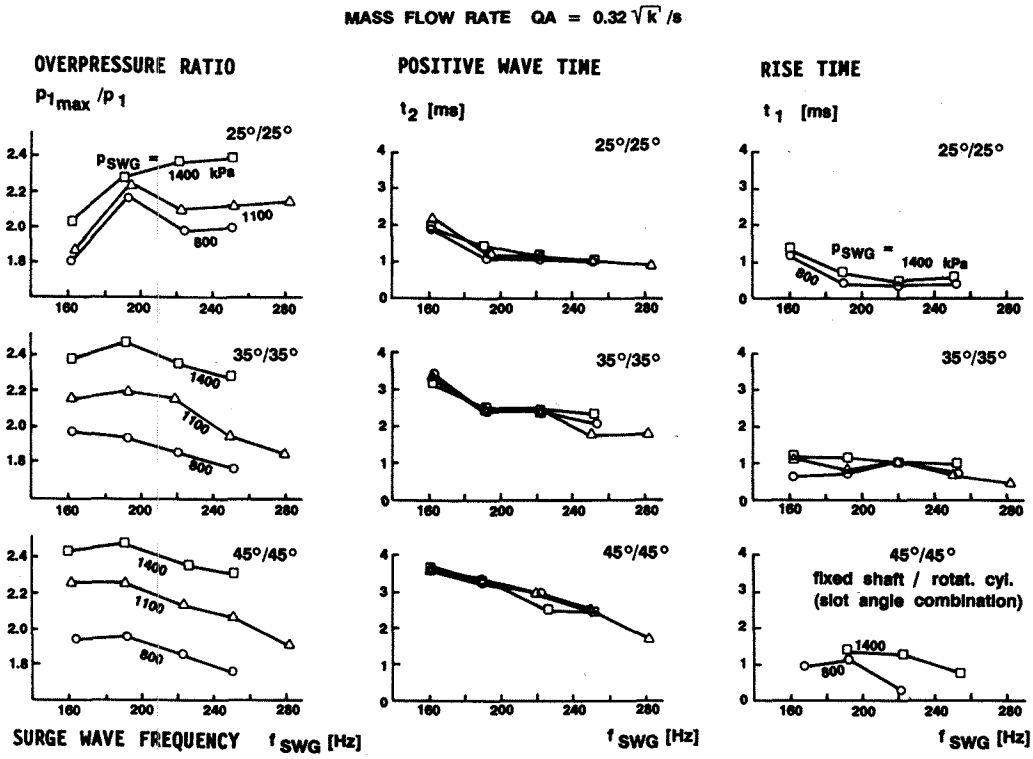

Fig. 24 Effect of parameter variation on overpressure ratio, positive wave time and rise time

left three diagrams overpressure ratio generally increases with increasing reverse flow pressure, as expected. However, the effect of reverse flow pressure on positive wave time (centre diagrams) and on rise time (right hand diagrams) was generally small except for the rise time with the 45°/45° slot angles.

The positive wave time can be essentially varied with surge wave frequency and slot angle. Positive wave time increases with increasing slot angle and declines with increasing valve frequency.

The rise time becomes slightly less with increasing surge wave frequency. The essential parameter to effect rise time is the slot angle. Shorter rise times are achieved by lower slot angles.

Combinations of different slot angles for the fixed shaft and the rotating cylinder were also tested (not shown in the figure), but had no noticeable effect, i.e. the surge wave shape is essentially dictated by the larger angle of either of the two cylinders.

A summary of the main results of the SWG calibration is given in Fig. 25. The overpressure ratio is predominantly dependent on the reverse flow pressure. At intake mass flow rates QA = 0.2 $\sqrt{K}$/s on overpressure ratio of 1.8 was achieved for all surge wave frequencies. When the intake mass flow rate increases, overpressure ratio is also increased. At QA = 0.32 $\sqrt{K}$/s overpressure ratios as high as 2.4 were achieved. These ratios were sufficiently high to simulate the surge waves produced by the engine considered.

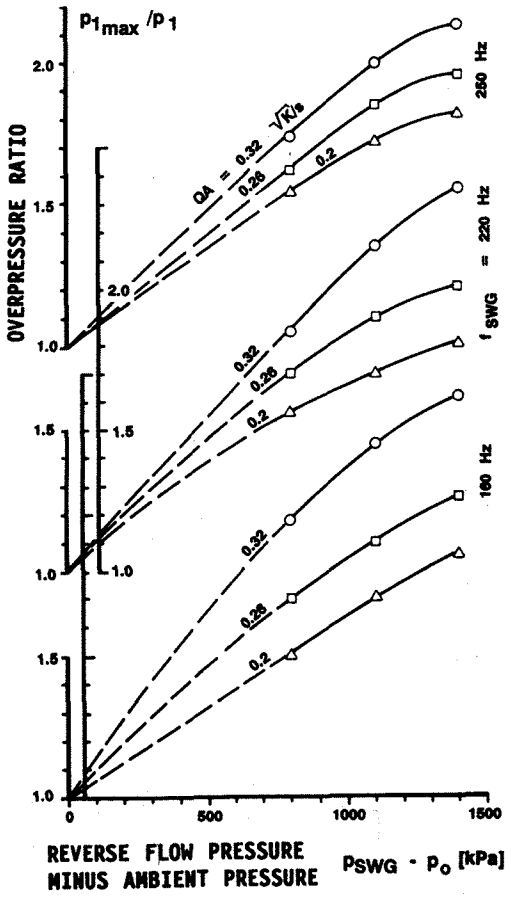

Fig. 25 Variation of overpressure ratio with reverse flow pressure and intake mass flow

4.4.3 Installation effects

Intake duct length

An investigation was made of the effect of the intake duct length on the surge wave parameters. The basic long duct representing the aircraft geometry was compared with a very short intake duct. The effect on the overpressure ratio is considerable (see Fig. 26). For the long duct there is only a small variation in the overpressure ratio with reverse flow pressure while for the short duct a steep rise in overpressure ratio with increasing reverse flow pressure can be noticed. The rise time is increased when the short duct is installed (see Fig. 27).

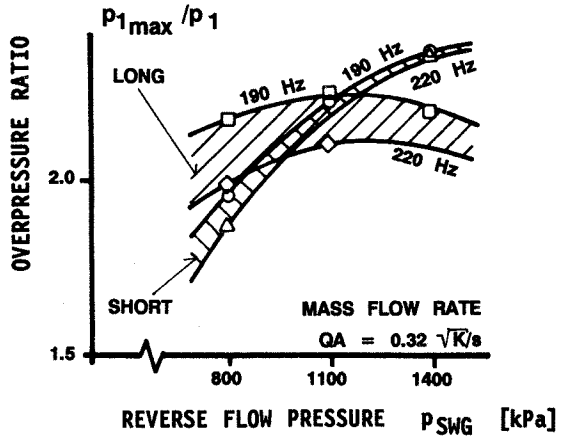

Fig. 26 Effect of intake duct length on overpressure ratio

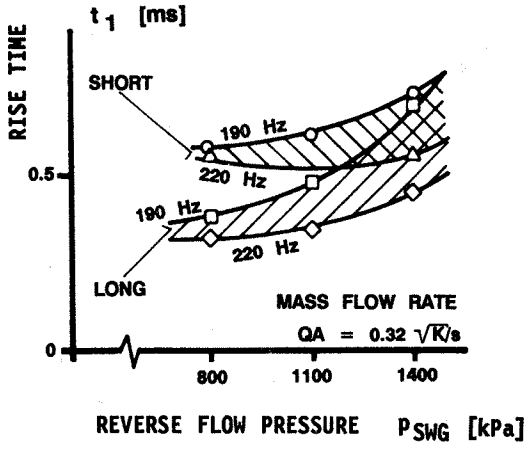

Fig. 27 Effect of intake duct length on rise time

The different surge wave signatures for the two duct lengths can be clearly seen in Fig. 28. The positive wave time is increased by about 40% for the short intake duct when compared with the long duct.

It can be concluded that the correct simulation of the intake duct geometry is essential when the SWG is being calibrated.

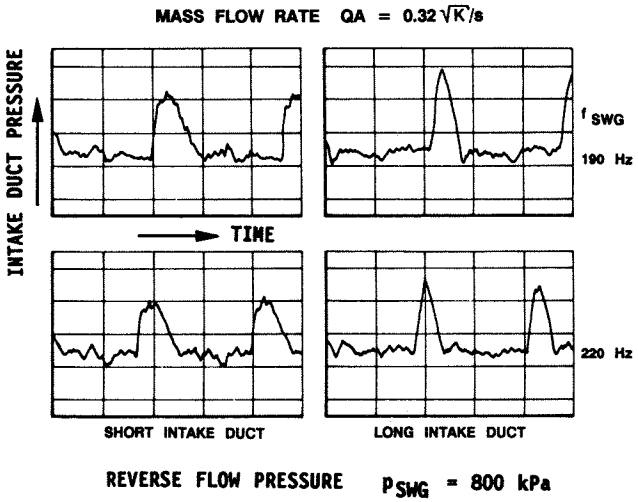

Fig. 28 Surge pressure wave signatures for two different intake duct lengths

AIP rake installation

Another installation effect was found due to the presence of the AIP rake ahead of the SWG. The rake is installed to measure intake duct swirl in the port duct of the intake model, as described in section 5.4. Fig. 29 shows that the overpressure ratio is reduced by about 0.1 to 0.2, depending on reverse flow pressure, when the rake is installed. Performance of surge simulation tests without the rake installed is therefore recommended so as not to alter the condition of the surge wave simulating an engine surge. When the rake is removed the risk of rake damage due to the heavy pressure waves created by the SWG is also reduced.

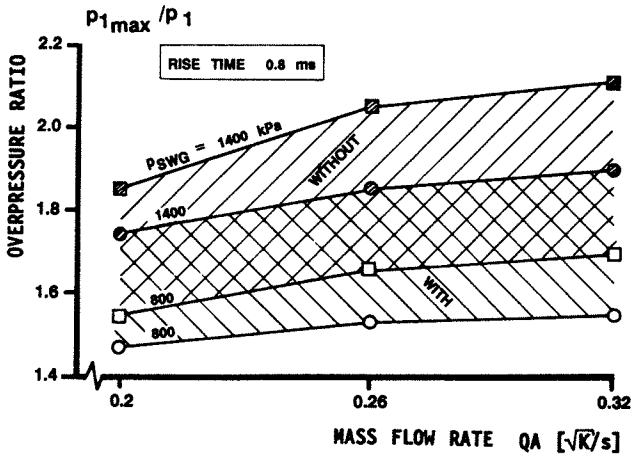

Fig. 29 Effect of AIP rake on overpressure ratio

Pressure supply tank

Initial tests with the burst diaphragm revealed that the pressure control valves in the reverse flow supply system were too slow to react to the sudden reverse flow demand. Shortly after the diaphragm had burst a breakdown of intake duct

pressure amplitudes to almost zero occurred (left-hand sketch in Fig. 30). The problem was completely solved by installation of a 1 m³ vessel very close to the SWG, i.e. adjacent to the tunnel test section. As can be seen in Fig. 30 (right-hand sketch) an almost constant maximum pressure amplitude could now be achieved when cyclic surges were initiated. Amplitudes varied by not more than 5%.

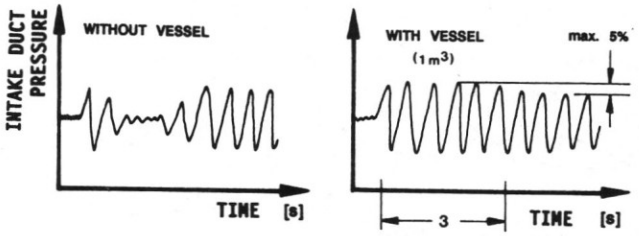

Fig. 30 Effect of pressure vessel installation on surge wave signature during initial cycles

5. SURGE SIMULATION IN AN INTAKE WIND-TUNNEL MODEL

5.1 Wind tunnel

The Transonic Wind Tunnel at DFVLR-AVA Göttingen (TWG) is a continuous (Göttingen-type) tunnel with a cross sectional area of 1m x 1m (see Fig. 31). The walls of the transonic test section (d in Fig. 31) - except the schlieren windows - are perforated to keep wall interferences small. In the subsonic range ($0.5 < Ma < 0.9$) the Mach numbers are controlled by an adjustable second throat diffuser (e). To achieve transonic velocities ($0.9 < Ma < 1.2$) and for boundary layer suction an auxiliary compressor is provided. For measurements at supersonic speeds ($1.3 < Ma < 2.0$) the model is mounted in the supersonic test section (c) and the Mach numbers are controlled by an adjustable Laval nozzle (b).

More detailed descriptions of the tunnel are given by Lorenz-Meyer (see Ref. 11).

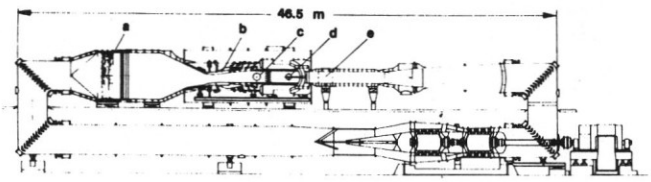

Fig. 31 Transonic wind tunnel at DFVLR Göttingen, TWG (1 x 1 m²)

5.2 Intake configuration

The intake configuration investigated consists of two two-dimensional, two shock, external compression inlets arranged closely side by side (see Fig.32). The inlet ramps have an effective wedge angle of 7° which adjusts the oblique shock on the cowl lips when the intakes are operated at the design Mach number. For boundary layer bleed

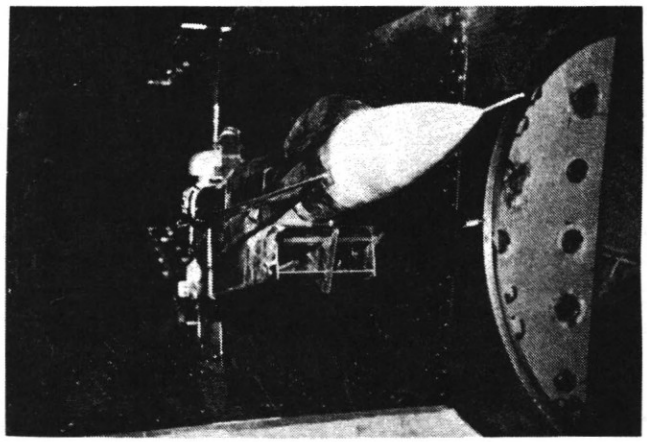

Fig. 32 Intake model installed in transonic wind tunnel

the ramp plates are perforated and the throat has a single slot (see Fig. 11). The two inlets are separated by an exchangeable splitter plate. To minimize disturbances due to separation of the inlet flow at high angles of attack the cowl lips swivel downward (see Fig. 11).

5.3 Model scheme

The overall model scheme is shown in Fig. 33. The model represents the front part (down to slightly behind the cockpit canopy) of a proposed twin-engined supersonic fighter airplane. It is fitted with a pair of foreplanes (see Fig. 32 to 34), the angle of incidence of which is adjustable

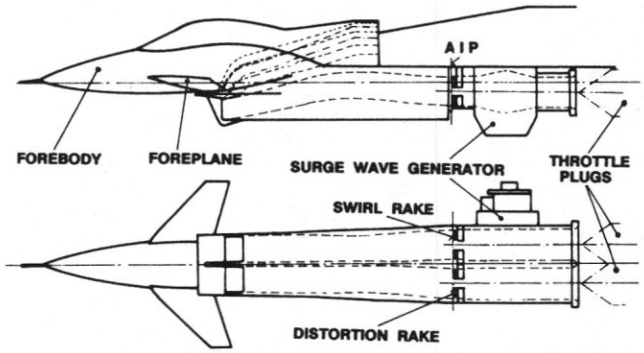

Fig. 33 Intake model scheme with surge wave generator

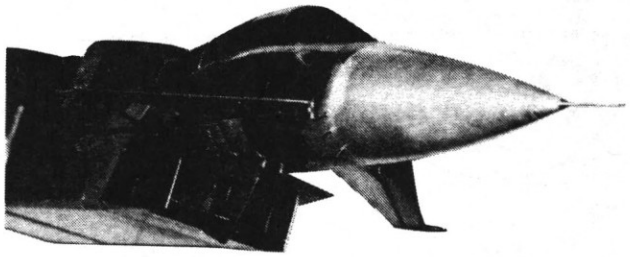

Fig. 34 Intake model

in seven steps between -40° and +10°. The inlets are placed close together under the belly. As one of the tasks of the measurements was to determine the optimum boundary layer bleed configuration, the bleed systems were designed for easy exchangeability of their main parts. Five ramp plates with four different perforation patterns and three throat slot inserts were provided. The mass flow of the bleed systems was adjustable by inserting different throttle nozzles into the bneed pipes, and was measured with the aid of Venturi nozzles. The SWG was installed in the port duct immediately downstream of AIP station. To investigate the influence of differently shaped splitter plates on surge wave propagation, five splitters with different sweep angles and leading edges were manufactured. Three pairs of side plates with corresponding shapes were provided, too. For performance measurements at high angles of attack it was possible to adjust the cowl lip angle θ_{VC} in eight steps from -30° to +10°. In addition, provisions were made to apply dummies of air data probes and antennae on the forebody.

More detailed descriptions of the model are given by Bass (Ref. 12) and by Scherbaum & Wolfrum (Ref. 13).

5.4 Instrumentation of the model

To determine the distributions of pitot pressure, swirl, and turbulence in the AIP two rakes were provided. The port rake (see Fig. 35) was equipped with 56 Pitot probes on eight arms at seven radii and with 16 five-hole probes (yaw meters) on eight additional arms at two radii which bore each a further Pitot probe. The starboard rake (see Fig. 35) is basically similar but its eight shorter arms were each fitted with one high-response pressure transducer (Kulite) at an intermediate radius and with another four Pitot probes instead of the yaw meters. Additionally at each rake three high-response pressure transducers were installed at the duct wall to measure fluctuating static pressures. From the distribution of Pitot pressure measured with the 72 (port) and 88 (starboard) probes not only the static distortion parameters were calculated, but also the mass flow rate was determined, which was adjusted with the aid of hydraulically-driven, computer-controlled mass flow plugs.

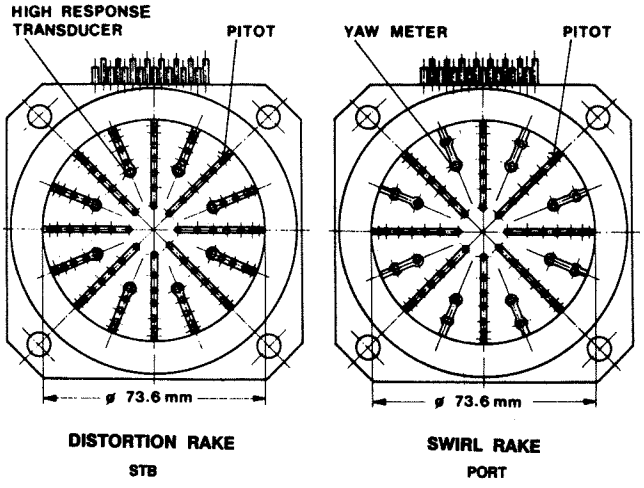

Fig. 35 Rakes installed at port and starboard aerodynamic interface planes

Information on the propagation of the surge wave was obtained by means of ten high-response pressure transducers mounted in each duct and another two at the forebody and the foreplane in front of the port inlet. The locations of the transducers are given in Fig. 36.

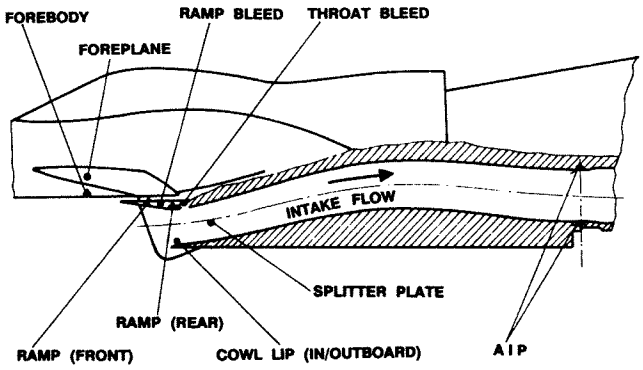

Fig. 36 Locations of high-response pressure transducers

5.5 Test programme

Static tests for surge interaction measurements were performed at the Calibration Tank Göttingen (ETG), see Ref. (14), and at subsonic and supersonic speeds in the TWG.

In the static case surge tests were carried out with intake mass flows between idle and maximum engine power setting. Different splitter plate shapes and cowl lip angles between 0° and -30° (deflected downwards) were investigated.

At subsonic flow velocities three different splitter plate configurations were investigated. Tests were performed at M_o = 0.6 and 0.8, angle of attack from -3° up to 15° and angle of side slip between +10° and -10°. The cowl lip was always deflected down to -30°.

At supersonic flows ($1.63 < M_o < 2.00$) two splitter plates were investigated with the cowl lip adjusted for maximum (flight) Mach number (θ_{VC} = 11.5°), and the unswept elliptical splitter additionally with datum cowl lip setting. The angles of attack in these investigations were α = -3°, 0° and 5° at β = 0°.

5.6 Test results (Ref. 15)

Pressure signatures from two typical cases in the TWG, one at M_o = 0.6 (Fig. 37) and the other at M_o = 1.8 (Fig. 38) have been selected from the large amount of recorded data. The signals were derived from the high-response pressure transducers at the model (Fig. 36). The traces from the subsonic test show a case where cyclic pressure waves were initiated by the burst diaphragm following a steady-state test period. The attenuation of the peak pressure level with upstream propa-

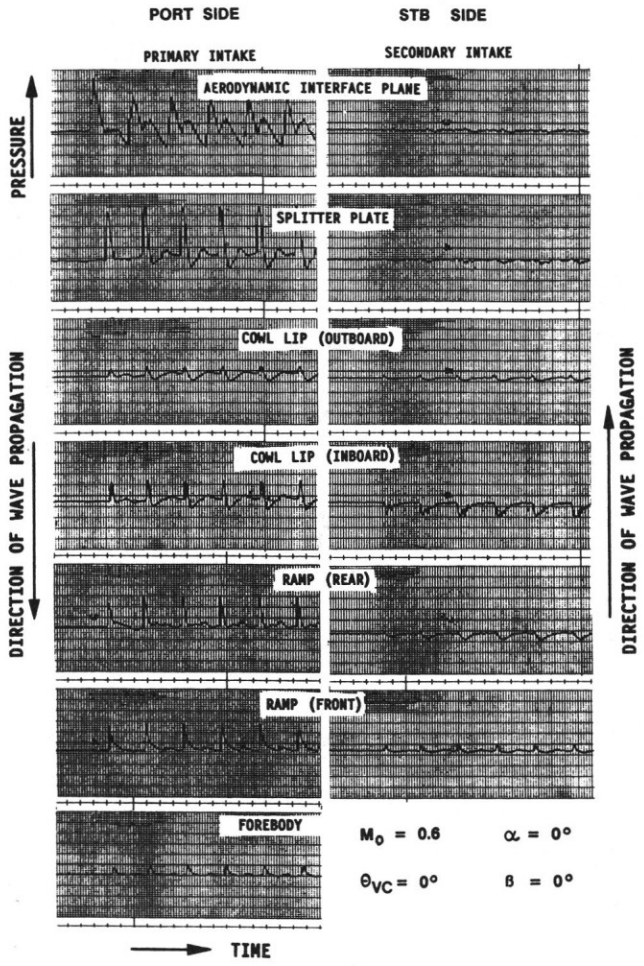

Fig. 37 Propagation of surge waves
M_o = 0.6

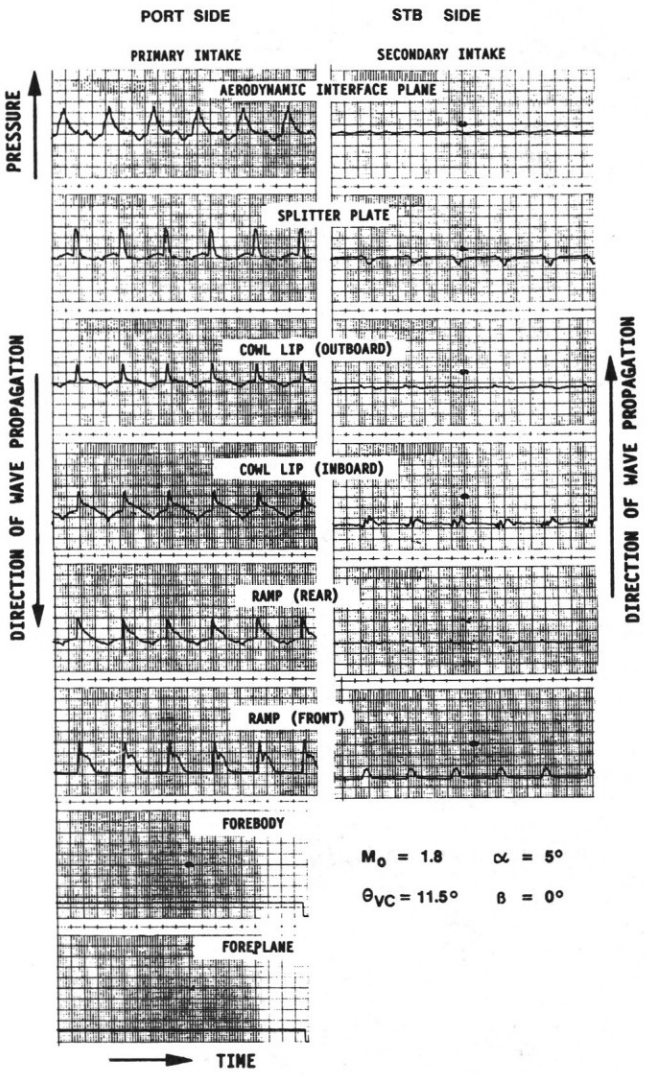

Fig. 38 Propagation of surge waves
M_o = 1.8

gation in the primary (port) forward intake can be seen clearly. As the wave is diffracted into the adjacent intake it is further attenuated. Pressure fluctuations at the AIP in the secondary intake are so low that they can hardly be identified. Small pressure fluctuations were observed at the lower side of the fuselage and foreplane.

At M_o = 1.8 (Fig. 38) a similar behaviour of wave propagation was observed. Of course, no disturbances occur at the forebody and foreplane at supersonic flight speeds.

The test results have shown that the typical aerodynamic intake paramters like

- o pressure recovery
- o turbulence
- o steady state and dynamic distortion

in the secondary intake were negligibly influenced by a surge in the primary intake.

Especially the dynamic distortion level - obtained by a synthesis method suggested by Borg (Ref. 16) - was well below the engine distortion limit.

6. REFERENCES

/1/ F.L. Marshall
Prediction of inlet overpressures resulting from engine surge
Journal of Aircraft, Vol. 10, No. 5, Mai 1973, pp. 274 - 278

/2/ P.J. Evans; P.O. Truax
YF-16 air induction system design loads associated with engine surge
Journal of Aircraft, Vol. 12, No. 4, April 1975, pp. 205 - 209

/3/ A.P. Kurkov; R.H. Soeder; J.E. Moss
Investigation of the stall hammer shock at the engine inlet
Journal of Aircraft, Vol. 12, No. 4, April 1975, pp. 198 - 204

/4/ K.W. Lotter; N.C. Bissinger
Dynamic pressure loads in the air induction system of the Tornado fighter aircraft
AGARD CP 248, 52nd PEP Meeting, Cleveland/Ohio, Oct. 1978

/5/ G. Patz
Stoßwellen in benachbarten Triebwerkseinläufen
ISL Report R 104/84, Febr. 1984

/6/ M.H. Marsden
The engine surge simulation unit of the wind tunnel department, BAe Filton Report WTM-1322 (12. March 82)

/7/ R. Scherbaum
Simulation von Stoßwellen in der Einlaufröhre des Concorde-Zwillingseinlaufmodells, Standversuch, Juli/Aug. 1982
Testphase 1 Band 1 und 2
MBB-Rep. TKF/R/39 (15. Dec. 1982)

/8/ R. Kern
Konstruktion und Bau eines Stoßwellengenerators, Oct. 86
MBB-Rep. ACA/R/21 (20. Nov. 1986)

/9/ R. Scherbaum
Erprobung des MBB-Stoßwellengenerators am Eichtank der DFVLR-Göttingen,
Testphase 1, Okt./Nov. 1983
MBB-Rep. ACA/R/018 (27. April 1984)

/10/ R. Scherbaum
Erprobung des MBB-Stoßwellengenerators am Eichtank der DFVLR-Göttingen,
Testphase 2, Feb./März 1984
MBB-Rep. ACA/R/019 (24. Nov. 1986)

/11/ W. Lorenz-Meyer
Der Transsonische Windkanal 1m x 1m der DFVLR-AVA. Nr. 4 in "Beiträge zur experimentellen Strömungsmechanik", Festschrift z. 65. Geburtstag von H. Ludwieg, DFVLR-AVA IB 251-77 A 37 (1977)

/12/ P. Bass
Model CC 12 specification. BAe, Aircr. Group, Warton Div., Rep. No. CC12/SPEC 1 (Febr.1984)

/13/ R.D. Scherbaum; G. Wolfrum
Specification of the data reduction for intake wind tunnel model CC 12, July 1984.
MBB-Rep. ACA/R/008 (30.7.84)

/14/ B. Binder; E. Melzer; R. Wulf
The New Calibration Tank for Engine Simulators at DFVLR Göttingen
AGARD-CP-348. pp 27-1 to 27-7

/15/ R. Scherbaum; G. Wolfrum
Surge interaction and performance tests with ACA intake model in the transonic and supersonic speed range at DFVLR-Göttingen, Mai 1984, Test phase 1

/16/ R. Borg
A synthesis method for estimating maximum instantaneous inlet distortion based on measured inlet steady state and RMS pressures
AGARD CP 301, Toulouse, Mai 1981, paper no. 19

/17/ C.P. Stocks; N.C. Bissinger
The design and development of the Tornado engine air intake
AGARD CP 301, Toulouse/France, May 1981, paper no. 10.